Wireless Pers Commun
DOI 10.1007/s11277-010-0116-3

AdaSynch: A General Adaptive Clock Synchronization Scheme Based on Kalman Filter for WSNs

Qiang Liu · Xue Liu · Jing Lun Zhou · Gang Zhou · Guang Jin · Quan Sun · Min Xi

Abstract Efficient and accurate clock synchronization is a challenge for wireless sensor networks (WSNs). Unlike previous works on clock synchronization in WSNs that consider communication delay as the main cause of clock inaccuracy, we propose a new adaptive synchronization scheme, AdaSynch, which considers the principium of the clock. We aim to overcome the challenges posed by WSNs' resource constraints such as limited energy and bandwidth, low precision oscillators and random factors. By implementing some experiments on *TelosB* platform, we find that the clock system switches between multiple clock models. Motivated by experiment results, we establish a general clock model which describes the clock offset in terms of the oscillators. We then design two kinds of basic Kalman filter models to achieve clock synchronization. In order to execute Kalman filtering, we propose a recursion method based on the Expectation-Maximization (EM) algorithm to access the parameters of the Kalman filter model adaptively. To describe alternation in the clock model, we propose a Multimodel Kalman filter, and put forward an adaptive method based on hypothesis testing to describe these complexities in the clock model. We demonstrate the performance gains of our scheme through experiments using different Kalman filter models based on experiment data.

Q. Liu (✉) · J. L. Zhou · G. Jin · Q. Sun
College of Information System and Management, National University of Defense Technology, 410073 Changsha, China
e-mail: qiangliu.mcgill@gmail.com

Q. Liu · X. Liu · M. Xi
School of Computer Science, McGill University, Montreal, QC, Canada

G. Zhou
Department of Computer Science, College of William and Mary, Williamsburg, VA, USA

Q. Sun
School of Industrial and Systems Engineering, Georgia Institute of Technology, Atlanta, GA, USA

M. Xi
Department of Computer Science, Xi'an Jiaotong University, Xi'an, China

Published online: 22 August 2010

Keywords Wireless sensor networks · Clock synchronization · Kalman filter · Hypothesis testing

1 Introduction

As a critical piece of infrastructure for any distributed system, clock synchronization has become an important and well-studied issue. As such, it is extremely important to wireless sensor networks (WSNs) [1–5]. For instance, many localization techniques measure the Time-Of-Flight (TOF), which is used to calculate distances by multiplying it with the medium propagation speed [6]. Another example is cooperative sensing nodes, which employ clock synchronization to determine a common time frame for configuring a beam-forming array or setting a Time Division Multiple Access (TDMA) radio schedule [5]. WSNs have many of the same requirements as traditional distributed systems: accurate timestamps are often needed in cryptographic protocols, coordinating scheduled events, ordering logged events for system debugging, and so on.

Many existing clock synchronization schemes, such as the widely used Network Time Protocol (NTP) for the Internet, are unsuitable for WSNs [7]. Classical clock synchronization schemes for wired networks assume that the system clock has high precision oscillators, and unbounded messages can be transmitted for synchronization. However, such assumptions are not appropriate for WSNs [4,8]. WSNs are representative example of resource-constrained networks because of battery supply, small size and low cost. Compared with the communication error for clock, all the characteristics of WSNs such as limitation, dynamicity, and randomicity become the key factor of clock out-of-synchronization, and make it difficult to carry out clock synchronization using existing schemes [2,8].

Some clock synchronization schemes that have been proposed mainly consider the clock offset caused by oscillator drift in the case of node to sink node. Under such schemes we can observe the fundamental reasons of clock non-synchronization caused by the special characteristics of WSNs. The most popular clock synchronization schemes use the stochastic differential equations (SDEs) to describe the clock model based on the physical characteristics of clock oscillators [9–11]. The constant model of clock skew with a "White noise" [12,13] often describes a relatively stable clock. The noise reflects stochastic effects such as phase noise. The first-order Gauss-Markov model, also known as the first-order Auto-Regressive (AR) model, is proposed to describe the time-varying clock skew in [2], and then a Kalman filter model built on the clock model is used to track the clock offset and skew. The schemes in [9] is modeled by the second-order model to describe the slope of the clock skew. However, most of these models can only describe a special situation for the clock skew. In real WSNs, the model of clock skew can follow different rules in different life periods [14]. In addition, the key of achieving the clock synchronization by SDEs for WSNs is the parameter estimation of the SDEs model. Unfortunately, getting accurate parameters is a difficult challenge.

These challenges of clock synchronization for WSNs call for new adaptive clock synchronization schemes. In this paper, we propose AdaSynch, an Adaptive clock synchronization schemes.

We first study the pattern of a sensor clock offset model. Some experiments using widely-used sensors are implemented to monitor the temperature of a certain area, and the experiments data of clock offset are collected.

Based on the analysis on the collected data, we design a general clock model in terms of the physical characteristics of the oscillators, which depicts the relation among offset, skew and skew aging rate accurately.

For the purpose of tracking the clock's offset and achieving clock synchronization, we leverage the Kalman Filter and propose an adaptive and real time parameter estimation method for the Kalman Filter based on the Expectation-Maximization (EM) algorithm. Note that Kalman Filter is an energy- and bandwidth-efficient clock synchronization techniques because it only needs to measure the clock readings in the synchronization [2]. Subsequently, experiments with different Kalman filter models are executed. The results show that the first-order and the second-order Kalman filter models can track the clock offset to an extent but there is still a gap between the experiment values and estimate values.

We also propose a Multimodal Kalman filter to close the gap between the experiment values and estimate values. We then design an adaptive model alternation method based on hypothesis testing to avoid calculation of transition matrix, which is hard to obtain but essential to the Multimodal Kalman filter. The tracking experiment based on experiment data shows that the Multimodal Kalman filter demonstrates superior performance than the first-order, second-order and ACES model [2] for clock synchronization.

In summary, the main contributions of this paper are as follows:

- To the best of our knowledge, we are the first to propose and implement a general adaptive clock synchronization scheme for WSNs in terms of the inherent nature of the clock.
- We propose a general clock model to describe the clock offset based on the physical characteristics of oscillators. The Kalman filter model is also proposed to achieve clock synchronization based on this general clock model.
- We apply the EM algorithm to address the problem of Kalman filter model parameter estimation. The advantage of this method is that it eliminates the need to provide parameters for the Kalman filter model because of the adaptivity.
- We establish a Multimodal Kalman filter which is adaptive based on hypothesis testing. The advantage of this Multimodel Kalman filter is can depict the alternation of multiple model and eliminate the subjectivity of adjudging the order of the Kalman filter model.

In the following sections, we show our analysis in detail. We first describe the experiment observations that motivate our works in Sect. 2. Section 3 presents the clock modeling based on experiment analysis. The motivation for this work is the experiment and data analysis, as well as the clock model we built according the experiment result. Section 4 presents the methodology for clock synchronization. Section 5 shows the Kalman filtering experiment step by step based on different Kalman filter models. Section 6 proposes the Multimodal Kalman filter based on hypothesis testing, and demonstrates the performance of the Multimodal Kalman filter based on experiment data. We conclude the paper in Sect. 7.

2 Motivation

To have a better understanding of clock synchronization for WSNs, we first analyze the resource constraint of sensor, and then implement extensive experiments to provide insights for guiding our clock synchronization.

2.1 Terminology

Before delving into the physics experiment of the sensor clock, we define the following terminology, which is consistent with existing definitions [8].

- Oscillator: An oscillator is an electronic device that generates a periodic electronic signal, which is often a sinusoidal waveform. In the real world, the sinusoidal is not pure because of the instability of frequency.
- Time: The time of a clock C in a machine is given by the function $C(t)$, where $C(t) = t$ stands for a ideal clock. t is an accurate real time standard like Universal Coordinated Time (UCT).
- Offset: Clock offset is the difference between the clock reading and the real time. The offset of clock C is given by $C(t) - t$.
- Skew: The skew of clock C is the slope of the change in offset compared to the ideal clock. The skew of clock C is given by $s(t)$.
- Aging rate: The aging rate of clock C is the first derivative of the clock skew value with respect to time, denoted $\gamma(t)$.

2.2 Resource constraint of sensor in WSN

For most current and future WSNs, sensors are resource-constrained. Pottie et al. [15] shows that transmitting 1 bit over 100 m requires 3 joules, which can be used for executing 3 million instructions. Because the sensors in WSNs are battery-powered, therefore, a successful synchronization scheme must minimize the amount of messages exchanged to preserve energy while maintaining high synchronization accuracy [2,14]. Scarcity of power on sensor nodes however is not the only resource constraint. The form-factor and low-cost constraints also lead to the use of low-precision oscillators in sensor nodes. The accuracy of clock readings derived from such oscillators are limited due to various reasons such as phase noise, thermal noise and aging. In addition, for many WSNs applications, sensors are often deployed in harsh environments. The temperature, humidity and vibration will affect the clock readings on sensors in terms of stochastic noise [4]. All the resource constraints cause that the classical clock model is unsuitable for WSNs.

2.3 Sensor clock experiment and analysis

Most clocks commonly used in WSNs are not precise, since the frequency of the oscillators is unstable such that time progression never exactly right. In fact, even a small frequency deviation in an oscillator, say 0.001%, would cause one second clock offset per day [13]. Compared with communication delay, clock offset originated from oscillator becomes the key factor of clock non-synchronization.

In an ideal world, $C(t) = t$ for all t, which means $s(t) = 0$. However, in resource-constrained WSNs, oscillators do not generate ideal periodic pulses. The oscillator's nonlinearity drift and phase noise make time progression inaccurate [13]. The characteristics of oscillator determine the behaviors of clock. To study the model of clock in terms of oscillator legitimately, we implement following experiments.

We examine the clock offset of ten wireless sensors with the same CPU host (2400 to 2483.5 MHz) and type (*TPR2400CA*) in the laboratory environments: a closed temperature (25 ± 5°C) controlled building with air-condition. All ten sensors are used to monitor the temperature of the building respectively, and set to send messages to a receiver at a constant interval (500 s). The receiver is connected to a computer driven by stable power. The receiving time of messages is the observation value of each sensor's clock reading. All the sensors are driven by the same kinds of fresh battery. Note that our experiments have been executed on sensor platform *TelosB*, and the sensors used in our experiment are the widely used product for real WSNs.

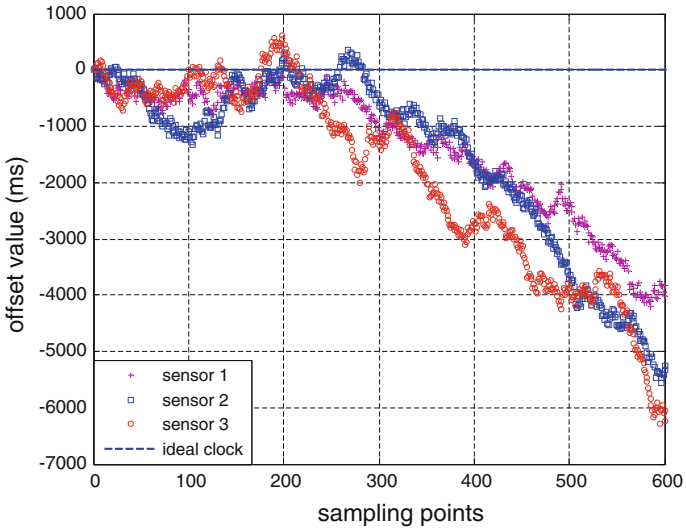

Fig. 1 Clock offset values of 3 clock sensors

We repeat the aforementioned experiment 20 times using 100 sensors. 100 sensors are divided into 10 groups in 10 sensors, and all the groups are taken to implement the experiment at the same time. By analyzing the collected data, we find that all the sensors have similar rules for clock offset. For simplicity, we take our experiment as an example, and randomly select three sensors' data to show the result of our analysis.

In this case, about 670 pieces of observation data of clock reading have been collected from each sensor until power depletion. Here we only take the first 600 data to study the clock model, since there is data leakage in the remaining lifespan of the batteries. Figure 1 shows the clock offset of three sensors varying with time. The dashed curve depicts the ideal clock. The other three curves stand for the clock offset of three sensors. From Fig. 1, it is clear that all the clock offset deviate away from the ideal curve with time, and the degree of deviation is growing. The former 300 sampling points are on relatively stable, and the classical clock model such as the first-order offset model (introduced in next section) can depict this situation properly. For the later 300 sampling points, there is an accelerated deviation from the ideal clock, and the classical clock model are unsuitable. In other words, there is a model "switch" in the process of life period. In addition, all of the information shown in Fig. 1 demonstrate that the clock offsets of three sensors are not stable with random noise.

To delve into the rule of sensor's skew, we make a liner fitting using the Least-Squares method for all the clock skews as shown in Fig. 2. From Fig. 2, we have three important observations. First, there are random perturbations for each clock skew. Second, the constant terms of these fitting curves are -9.629×10^{-6}, -9.3105×10^{-6} and -9.5524×10^{-6} ms. They are very closed to each other and 0 but less than 0. Third, the first-order term of these fitting curves all have the 10^{-9} order of magnitude coefficient. According to these observations, it is clear that our clocks are slow, and the clock skew of our experiment takes on the degradation trend with almost the same initial value (less than but closed to zero) and degradation rate. In addition, the random noise exists during the whole process.

Without loss of generality, we execute the similar experiments in different environments such as high temperature and humidity using different sensors. By analyzing the data, we

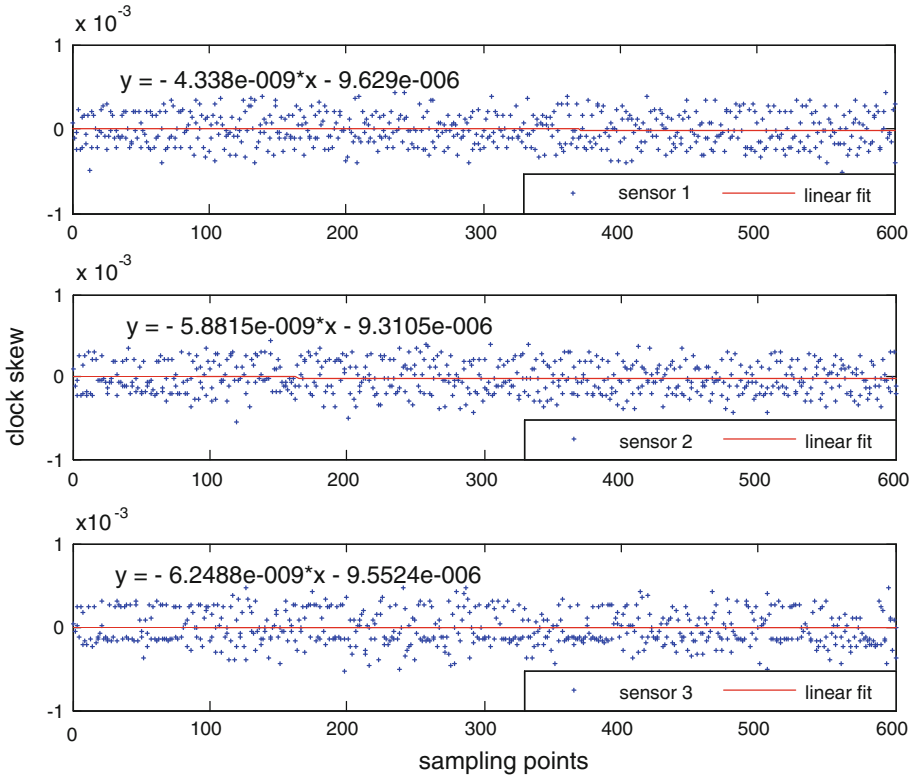

Fig. 2 Clock skew values of 3 clock sensors

find that most of the sensors have the "switch" phenomenon, and the environment just take affect on the skew of clock. The result is consistent with the view as shown in the second figure of [1]. Note that we do not think that all the sensors have the "switch" phenomenon. We just take the "switch" case to delve into the general clock model which is compatible with the "switch".

In short, we summarize the conclusion as follows:

- As a typical clock of WSNs, the classical clock model is unsuitable, and we should take the clock skew, aging rate and noise into consideration for the clock synchronization scheme in terms of oscillator.
- A simple and single model cannot describe the clock of real WSNs in some of cases.

3 Clock Modeling

The complex rule of clock offset motivate us to delve into the clock model so that we make an efficient clock synchronization for WSNs. The key of a clock is the frequency of oscillator which affect the performance of the clock directly. In this section, we study the clock model in terms of oscillator. We first state the classical clock model, and then propose a general clock model which can describe the complex case of clock based on the classical clock model.

3.1 Classical Clock Model

According to the principium of clock, instantaneous clock offset $o(t)$ at time t can be described by using the instantaneous clock skew $s(\tau)$, the initial clock offset o_0 and the random noise $\omega(t)$ as follows [2]:

$$o(t) = \int_0^t s(\tau)d\tau + o_0 + \omega(t), \tag{1}$$

where τ is the given interval.

This is a classical continuous-time general clock offset model with the form of random process. The integration reflects the varying of offset induced by oscillator, and the noise reflects the random physical effects such as the random error of counter and power of battery. It is straightforward to reflect the generality rule of the clock in the real world.

In the real world, the observation data takes on the discrete-time state by sampling. Therefore, the continuous-time model can be expressed in the form of discrete-time model based on Eq. (1) as:

$$o[n] = \sum_{k=1}^{n} s[k]\tau[k] + o_0 + \omega[n], \tag{2}$$

where k is the index of sample, $\tau[k]$ is the sampling interval at the kth sample. It is clear that this model is very general, since the interval of each sampling can choose different values and the $\omega[n]$ is a random noise. The kinds of random noises vary from clock to clock. The random noises $\omega[n]$ is generally described in time domain by white noise which is a independently Gaussian process with zero mean and variance σ_ω^2. Equation (2) can be rewritten into a recursive form as:

$$o[n] = o[n-1] + s[n]\tau[n] + \nu[n], \tag{3}$$

where $\nu[n]$ is also a white noise. Note that it is not difficult to verify $\sigma_\nu^2 = 2\sigma_\omega^2$ based on the relation $\nu[n] = \omega[n] - \omega[n-1]$.

For model Eq. (3), two classes of assumptions: constant skew and independent skew [2,12] are commonly applied. However, these two classes of skews are too simple because neither of them consider any statistical and dependent characters. For the simple case, if the clock has no "switch" phenomenon, the classical model is suitable; However, from our experiment, we clearly see that the skew time-series has the liner relation and random noise adhering the series in Fig. 2. In addition, the model "switch" can be found in Fig. 1. Therefore the classical clock model is not suitable for the case of our clock.

3.2 A General Clock Model Based on Practical Experiment

To depict the accelerated deviation from the ideal clock shown in Fig. 1, we delve into the clock skew model from the oscillator's characteristics, and then built a general clock model.

The clock skew is determined by two factors: the inherent frequency of oscillator and the phase noise. The output of a perturbed oscillator can be given by $V(t) = V_0 cos[2\pi f_0 t + \phi(t)]$ [2,9], where $V(t)$ is the instantaneous voltage of oscillator, V_0 is the amplitude of frequency, f_0 is the inherent frequency, $\phi(t)$is the phase noise. The phase noise $\phi(t)$ affects the frequency of oscillator $\frac{1}{2\pi f_0}\frac{d\phi(t)}{dt}$. If the frequency has a variance rate V_f, the instantaneous of clock frequency can be described as:

$$f(t) = \int_0^t V_f(\tau)d\tau + f_0 + \frac{1}{2\pi f_0}\frac{d\phi(t)}{dt}. \tag{4}$$

Because clock skew can be mapped to the frequency of oscillator [2], the relation of Eq. (4) can be converted to describe clock skew as:

$$s(t) = \int_0^t \gamma(\tau)d\tau + s_0 + \eta(t), \tag{5}$$

where aging rate of skew $\gamma(\tau)$, initial clock skew s_0 and skew noise $\eta(t)$ correspond to $V_f(\tau)$, f_0 and $\frac{1}{2\pi f_0}\frac{d\phi(t)}{dt}$ respectively.

Similar to Eq. (2), the instantaneous clock skew $s[n]$ at nth sample can be written in discrete-time model as:

$$s[n] = \sum_{k=1}^{n} \gamma[k]\tau[k] + s_0 + \eta[n], \tag{6}$$

where $\gamma[k]$ is the aging rate, s_0 is the initial clock skew, and $\eta[n]$ is the additive noise.

Similar to Eq. (3), we rewrite the instantaneous clock skew using the recursive form as:

$$s[n] = s[n-1] + \gamma[n]\tau[n] + \xi[n], \tag{7}$$

where $\xi[n]$ is a white noise, and $\sigma_\xi^2 = 2\sigma_\eta^2$. Note that our discrete-time skew model is quite general. For the relatively stable oscillator, we think the aging rate equals to 0, and then the model can describe the constant skew with additive noise. In contrast, the aging rate equals to a constant rather than 0 or another value varying with time, and our model is still qualified.

Combining Eq. (3) with Eq. (7), we build a general model for clock offset like the accelerated motion model as:

$$o[n] = o[n-1] + s[n]\tau[n] + \frac{1}{2}\gamma[n]\tau^2[n] + \vartheta[n], \tag{8}$$

where $\vartheta[n]$ is the combination of offset noise, skew noise and aging noise. If ignoring the aging rate, this model corresponds to the classical model.

In our paper, we think that a constant or zero is appropriate for the aging rate of skew, since the polynomial fitting curve of the first-order difference of skew for three sensors all has two items including a constant item and the first-order item with more than 10^{-50} order coefficient. From our experiment, the rule of the former 300 points accord with the classical model, and the later 300 points can be expressed by our model with a constant or zero aging rate of skew. In next section, we build the clock synchronization scheme based on our model.

4 Methodology for Clock Synchronization

By tracking the clock offset, we can achieve the clock synchronization effectively [2,10,11]. Kalman filter is an efficient recursive tracking method that estimates the state of a linear dynamic system from a series of noisy measurements [16–18]. In this section, we design two kinds of Kalman filters to track the time-varying clock offset based on the proposed clock model. We first construct the Kalman model for the clock, and then propose an adaptive parameter estimation method to obtain the parameters of the Kalman model.

4.1 Kalman Filter Model for Clock

We define the Kalman filter for clock based on the proposed model as:

$$\begin{aligned} x[n] &= Fx[n-1] + \mu[n] \quad \text{state equation} \\ y[n] &= Hx[n] + \zeta[n] \quad \text{observation equation,} \end{aligned} \tag{9}$$

where $x[n]$ is the nth state variables of clock; $y[n]$ is the nth observation variables of clock; F is the state transition model which is applied to the previous state $x[n-1]$; H is the observation model which maps the true state space into the observed space; $\mu[n]$ and $\zeta[n]$ are the white noise with covariance Q and R respectively.

Furthermore, we define two kinds of Kalman filter models in terms of aging rate.

- *Case* I: When the aging rate equals to 0, the clock model can be considered as a uniform motion model. From Eqs. (3) and (7), we set Kalman filter as: $x = [o[n]\ s[n]]'$, $F = \begin{bmatrix} 1 & \tau \\ 0 & 1 \end{bmatrix}$, $H = [1\ 0]$. In addition, the state noise is $\mu[n] = [\vartheta[n]\ \eta[n]]'$, and the observation noise is $\zeta[n]$, where $[\cdot]'$ is the transpose of a matrix. This is the first-order Kalman filter in terms of clock offset.
- *Case* II: When the aging rate equals to a constant rather than zero, the clock model can be considered as an accelerated motion model. Here we consider the aging rate as a random process with a small perturbation around the mean. Assume the small perturbation is a white noise, we set Kalman filter as: $x = [o[n]\ s[n]\ \gamma[n]]'$, $F = \begin{bmatrix} 1 & \tau & \tau^2/2 \\ 0 & 1 & \tau \\ 0 & 0 & 1 \end{bmatrix}$, $H = [1\ 0\ 0]$. In addition, the state noise is $\mu[n] = [\vartheta[n]\ \eta[n]\ \rho[n]]'$, and the observation noise is $\zeta[n]$, where $\rho[n]$ is the noise of aging rate. This is the second-order Kalman filter in terms of clock offset.

No matter what kind of Kalman filter model is used, the key of Kalman filter tracking is the parameter estimation. However, the parameter estimation of Kalman filter is a challenging problem for real systems. In order to address this challenge, we present an adaptive and real-time parameter estimation method in next section.

4.2 Adaptive Parameter Estimation Method Based on EM Algorithm

For Kalman filter model, the state variables of system are unobserved. The classical method such as Maximum Likelihood Estimate is not suitable for our case. In this paper, we apply the EM algorithm to solve this problem, since the EM algorithm is efficient for finding maximum likelihood estimation of parameters in probabilistic models, where the model depends on unobserved latent variables [19,20].

4.2.1 EM Algorithm for Kalman Filter

Assuming a sequence of N observation data vectors $(y_1, y_2, \ldots, y_N)$ is denoted by $\{y\}$; similarly for the states.

According to the Markov property of Kalman filter model, we get the joint probability of state variables $\{x\}$ and observation variables $\{y\}$ as:

$$p(\{x\},\{y\}) = p(x_1)\prod_{i=2}^{N} p(x_i\,|x_{i-1}\,)\prod_{i=1}^{N} p(y_i\,|x_i\,), \tag{10}$$

where $p(\cdot)$ is the probability function, x_1 is the initial state.

We can compute the conditional densities for the state and observation as:

$$\begin{aligned} p(x_i\,|x_{i-1}\,) &= \exp\left\{-\frac{1}{2}[x_i - Fx_{i-1}]' Q^{-1}[x_i - Fx_{i-1}]\right\} \\ &\quad \cdot (2\pi)^{-k_1/2}\,|Q|^{-1/2}\,, \end{aligned} \tag{11}$$

$$\begin{aligned} p(y_i\,|x_i\,) &= \exp\left\{-\frac{1}{2}[y_i - Hx_i]' R^{-1}[y_i - Hx_i]\right\} \\ &\quad \cdot (2\pi)^{-k_2/2}\,|R|^{-1/2}\,, \end{aligned} \tag{12}$$

where k_1 and k_2 are the dimension of state variables and observation variables, respectively.

The joint log probability function can be expressed as a sum of polynomials,

$$\begin{aligned} \log p(\{x\},\{y\}) = &-\sum_{i=1}^{N}\left(\frac{1}{2}[y_i - Hx_i]' R^{-1}[y_i - Hx_i]\right) \\ &-\sum_{i=2}^{N}\left(\frac{1}{2}[x_i - Fx_{i-1}]' Q^{-1}[x_i - Fx_{i-1}]\right) \\ &-\frac{N}{2}\log|R| - \frac{N-1}{2}\log|Q| + constant, \end{aligned} \tag{13}$$

where *constant* is probability of initial state x_1.

However, the state variables play an unobserved role in real world, and we can not achieve the parameter estimation by maximizing above joint log probability function directly based on Maximum Likelihood Estimate method (MLE). In our case, instead of maximizing Eq. (13), we use the EM algorithm to maximize the following conditional expectation log likelihood:

$$\Theta = E[\log p(\{x\},\{y\}\,|\{y\})], \tag{14}$$

where $E[\cdot\,|\cdot]$ is the conditional expectation function. The execution of Eq. (14) is the E-step of EM algorithm.

According to the results in [20], we get the estimation by taking the corresponding partial derivative of the conditional expectation log likelihood:

$$Q = \frac{1}{N-1}\left(\sum_{i=2}^{N} P_i - FP_{i-1,i} - P_{i,i-1}F' + FP_{i-1}F'\right), \tag{15}$$

$$R = \frac{1}{N}\left(\sum_{i=1}^{N} y_i y_i - 2H\hat{x}_i y_i' + HP_i H'\right), \tag{16}$$

where $\hat{x}_i = E[x_i\,|\{y\}]$, $P_i = E[x_i x_i'\,|\{y\}]$ and $P_{i,i-1} = E[x_i x_{i-1}'\,|\{y\}]$. The execution of Eqs. (15) and (16) is M-step of EM algorithm.

4.2.2 Technical Realization for EM Algorithm

In order to calculate the values of Q and R, we need to obtain the value of $\hat{x}_i$, P_i and $P_{i,i-1}$. In this section, we use the Kalman filter iteration to solve this problem.

For a real time system, given N pieces of observation data, we get the estimation of state at ith iteration as follows [16]:

$$x_{i,i-1} = Fx_{i-1,i-1}, \tag{17}$$

$$V_{i,i-1} = FV_{i-1,i-1}F' + Q_i, \tag{18}$$

$$K_i = V_{i,i-1}H_i'(H_iV_{i,i-1}H_i' + R_i)^{-1}, \tag{19}$$

$$x_{i,i} = x_{i,i-1} + K_i(y_i - H_ix_{i,i-1}), \tag{20}$$

$$V_{i,i} = (I - K_iH_i)V_{i,i-1}, \tag{21}$$

where $x_{i,i-1}$ is the estimation of the state at time i given observations up to and including time $i-1$, $V_{i,i-1}$ is the error covariance matrix of state (a measure of the estimated accuracy of the state estimate), similarly for $x_{i,i}$ and $V_{i,i}$, and K_i is the optimal Kalman gain.

It is clear that the estimation of state is a forward recursion. The $\hat{x}_i = x_{i,N}$ is the minimum mean square error estimation of x_i given all observation data. It is similar with the P_i.

In order to calculate $\hat{x}_i$ and $P_i = V_{i,N} + x_{i,N}x_{i,N}'$, we use a backward recursion shown in [19] as:

$$J_{i-1} = V_{i-1,i-1}F(V_{i,i-1})^{-1}, \tag{22}$$

$$x_{i-1,N} = x_{i-1,i-1} + J_{i-1}(x_{i,N} - Fx_{i-1,i-1}), \tag{23}$$

$$V_{i-1,N} = V_{i-1,i-1} + J_{i-1}(V_{i,N} - V_{i,i-1})J_{i-1}'. \tag{24}$$

In addition, we also require $P_{i,i-1} = V_{i,i-1}^N + x_i^N(x_{i-1}^N)'$, which can be obtained through the backward recursions for $i = N, N-1, \ldots, 1$ as:

$$V_{i-1,i-2}^N = V_{i-1,i-1}J_{i-2}' + J_{i-1}\left(V_{i,i-1}^N - FV_{i-1,i-1}\right)J_{i-2}', \tag{25}$$

where Eq. (25) is initialized $V_{N,N-1}^N = (I - K_NH)FV_{N-1,N-1}$.

4.2.3 Adaptive and Real-Time Iteration for Kalman Filtering

The sections above propose a method to obtain the value of Q and R. In this section, we propose an iteration algorithm for adaptive and real-time estimating value of Q and R. As shown in Fig. 3, it is an adaptive recursion method. Given l pieces of observation data, we first use the Kalman forward recursion to obtain the state $x_{i,i}$ and covariance $V_{i,i}$, and then use the Kalman backward recursion to obtain the $\hat{x}_i$, P_i, $P_{i,i-1}$, where $i = 1, 2, \ldots, l$. Therefore, we get the function of the conditional expectation Θ. This is the process of E-step of EM algorithm. The M-step of the EM algorithm is to maximize the function Θ, and we get the estimation of Q and R. By iterating the E-step and M-step, we adaptively track the clock given only observation data in real time.

5 Clock Tracking Using Adaptive Parameter Estimation

In this section, we implement the tracking experiments based on three sensors' data to examine the performance of the two kinds of basic Kalman filter models.

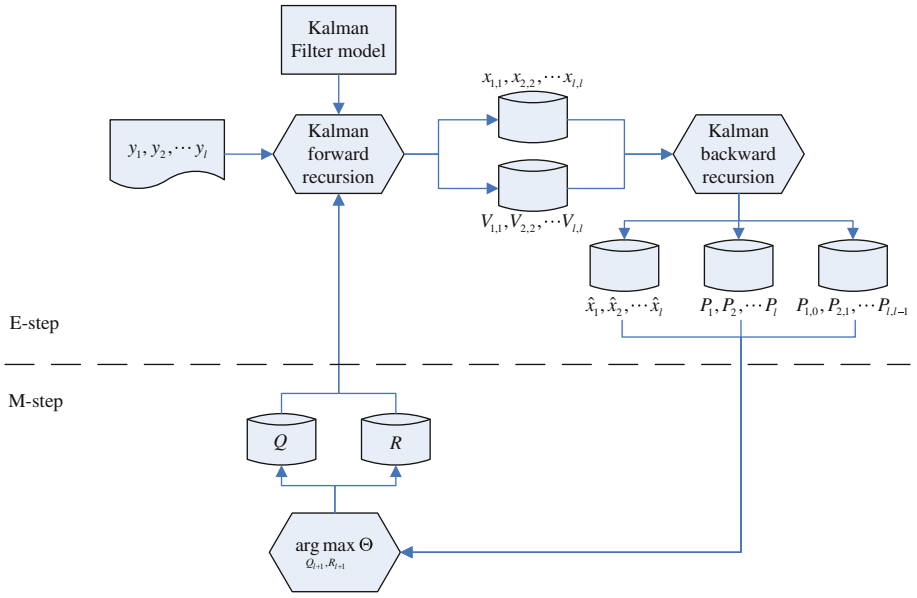

Fig. 3 A flow sheet of adaptive parameter estimation

5.1 Clock Tracking Using the First-Order Model

To demonstrate the Kalman filter's tracking performance for our clocks, we first implement a tracking experiment based on the first-order model shown in *Case* I in this section.

In our experiment, the interval of sampling is fixed at $\tau[n] = 500$ s. In addition, the aging rate equals to 0 because we are ignoring the aging rate. In this case, given $N1(N1 > 2)$ observation data for learning the parameters, we initialize the Kalman filter as:

$$\begin{aligned} x_{1,1} &= [o[1] \;\; s[1]]' \\ V_{1,1} &= diag[var[\{o[i]\}] \;\; var[\{s[i]\}]], \quad (i = 1, \ldots, N1), \\ Q_1 &= diag[c_1 \;\; c_2], \quad R_1 = c_3, \end{aligned} \tag{26}$$

where var[·] is the variance function. $diag[\cdot]$ is the diagonal matrix function. $\{\cdot\}$ is a data set.

A list of examples are implemented to profile this case. According to Eq. (3), we set $c_1 = var[diff[\{o[i]\}]]$, since the skew values are far less than offset values, where $diff[\cdot]$ is the difference function. Following the same reason as c_1, we set $c_2 = var[diff[\{s[i]\}]]$, $c_3 = var[\{o[i]\}]$. Here we denote these initial conditions as G_0. In addition, in order to verify the stability of the Kalman filter in terms of initial condition, we reset these initial conditions by multiplying a factor of 0.01 and 100 respectively, and we denote the two groups of new initial conditions as G_1 and G_2. In Fig. 4, we show the estimation of Q and R obtained by the EM algorithm. $Q1$ is the variance of offset noise, and $Q2$ is the variance of skew noise. It is clear that the estimation does not strongly depend on the initial conditions, and converges to a stable value in a short time. Note that we only show the first 40 sampling points, since later points are convergent.

In Fig. 5, we show the Kalman filter tracking for three sensors using the initial condition G_0 for simplicity. We can see that the Kalman filter track the offset in the first 300 points very closely. The estimation deviation from the observation curve increases with time. We

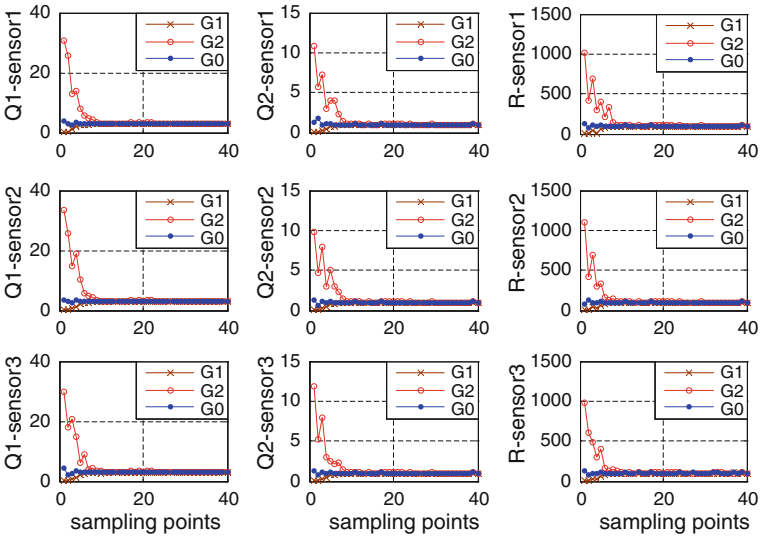

Fig. 4 Adaptive estimation of Q and R based on the first-order model

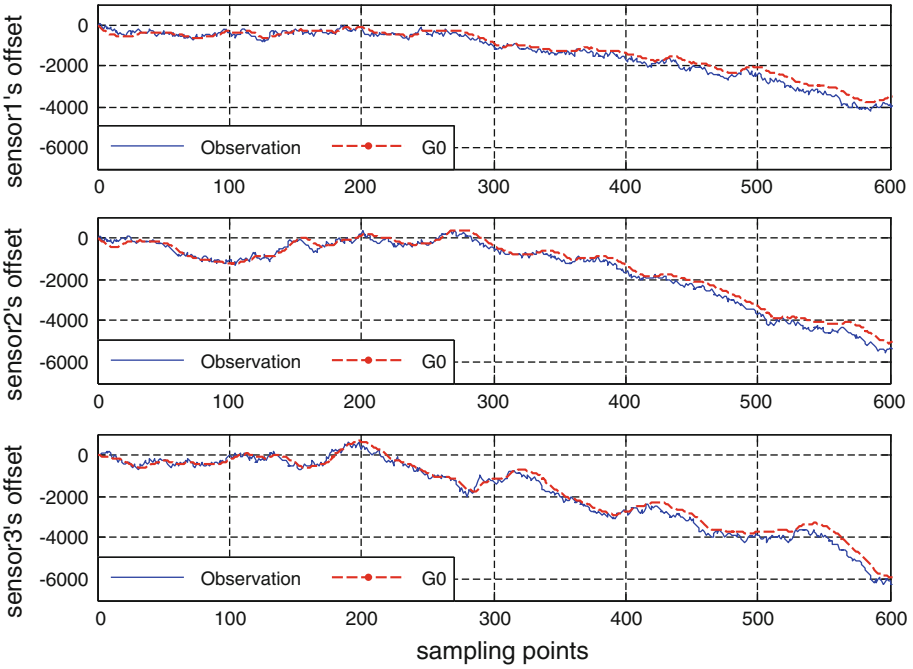

Fig. 5 Tracking of clock offset using the first-order model

evaluate the performance of the tracking by means of an error covariance matrix which is a measure of the estimated accuracy of the state estimation. From Fig. 6, we can see that the first entry of the matrix ($P(1, 1)$) reaches a stable value in a short time for the three sensors before the 300 points. However, $P(1, 1)$ takes on a growth trend for the later points.

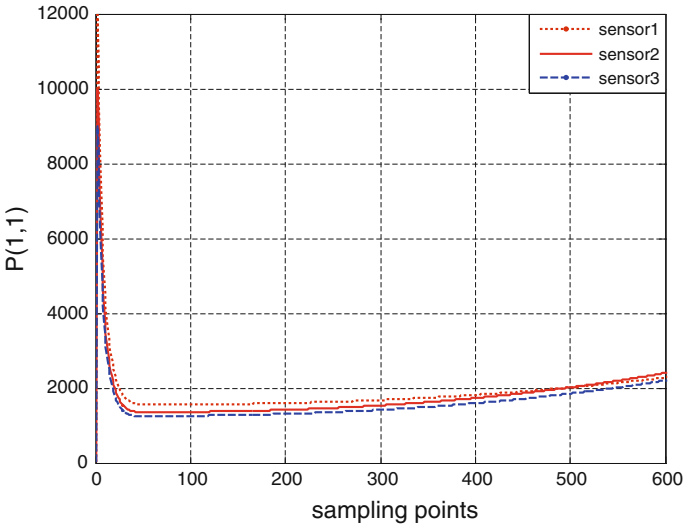

Fig. 6 The first entry of the error covariance matrix of clock offset tracking by using the first-order model

In short, we make the following conclusions. First, the EM algorithm for estimating Q and R is insensitive to the initial condition. Second, the Kalman filter shown in $Case$ I can only track the clock offset for some points. This is reasonable because there is an aging trend for later points.

5.2 Clock Tracking Using the Second-Order Model

In this section, we implement an experiment to track the clock offset using the model shown in $Case$ II. In this case, we initialize the Kalman filter in the same way as the previous section:

$$\begin{aligned} x_{1,1} &= [o[1]\ \ s[1]\ \ \gamma[1]]' \\ V_{1,1} &= diag[var[\{o[i]\}]]\ \ var[\{s[i]\}]]\ \ var[\{\gamma[i]\}]] \\ Q_1 &= diag[c_4\ \ c_5\ \ c_6], \quad R_1 = c_7. \end{aligned} \tag{27}$$

Similar to the previous section, the skew and aging rate values are far less than offset values, we set initial values as $c_4 = var[diff[\{o[i]\}]]$, $c_5 = var[diff[\{s[i]\}]]$, $c_6 = var[diff[\{\gamma[i]\}]]$, $c_7 = var[\{o[i]\}]$. Here we denote these initial conditions as G_0. Just like the previous section, we reset these initial conditions by multiplying a factor of 0.01 and 100 respectively, and we denote the two groups of new initial conditions as G_1 and G_2. By implementing the experiment, we find that Q and R estimated by EM algorithm are very similar to Fig. 4, where Q and R converge to a stable value in a short time. Therefore, we do not show the detailed figure here. Figure 7 shows the tracking situation of offset using the second-order model. We can see that the Kalman filter cannot track the offset closely at the first 300 points, but there is satisfactory tracking at later points. From Fig. 8, we can see that the first entry of the matrix do not converge to a stable value until about the 300th point for all three sensors. This indicates that the second-order model is only accurate for tracking later points.

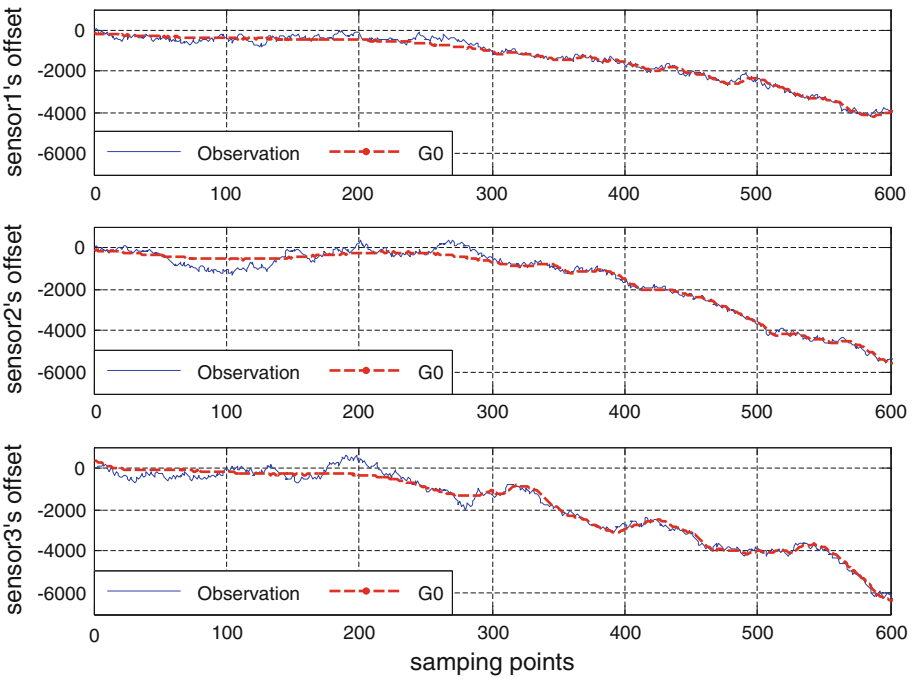

Fig. 7 Tracking of clock offset using the second-order model

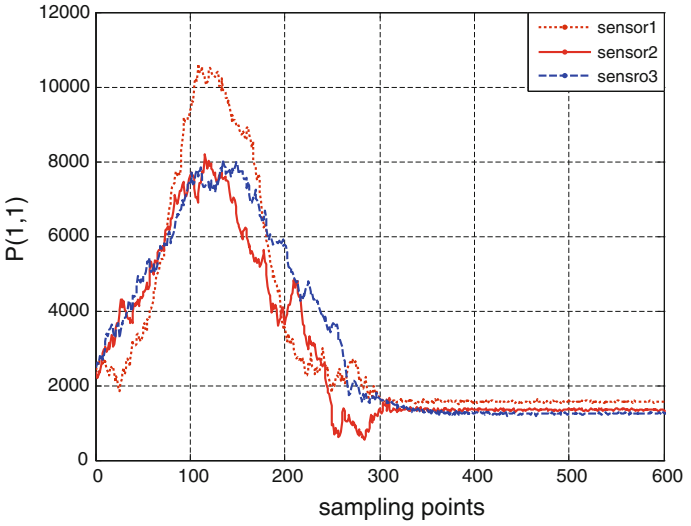

Fig. 8 The first entry of the error covariance matrix of clock offset tracking by the second-order model

6 Multimodel Kalman Filter for Clock Tracking based on Hypothesis Testing

According to the experiments above, we can understand that neither the first-order nor the second-order model alone can track our clock offset during the whole life period.

Furthermore, we can learn that the first part of points follow the first-order model, and later points follow the second-order model. In this section, we propose a Multimodel Kalman filter consisting of the first-order model and the second-order model to track the clock offset. In the Multimodel, the state of a dynamic system with the two behavior models can "switch" from one to another.

Interacting Multiple Model (IMM) is an effective method for the clock model alternation case [21,22]. However, the key requirement of the IMM is to obtain the transition probability matrix. For a clock with clock model alternation case, it is very difficult to get the transition probability matrix, and the IMM filter is not suitable for clock synchronization. In order to address this issue, we propose an adaptive Multimodel Kalman filter scheme based on hypothesis testing to achieve the model alternation.

6.1 Hypothesis Test for Multimodel Kalman filter

From the iteration of Kalman filtering, we get the observation residue U_i and residue covariance S_i at the ith observation as:

$$\begin{aligned} U_i &= y_i - H_i x_{i,i-1} \\ S_i &= H_i V_{i,i-1} H' + R_i, \end{aligned} \tag{28}$$

Using the variables shown in Eq. (28), we define the statistic D_i as the following:

$$D_i = U_i' S_i^{-1} U_i. \tag{29}$$

Because the observation residue U_i follows Gaussian distribution, the statistic D_i follows Chi-square distribution with m degrees of freedom, where m is the dimension of U_i. For a system with two kinds of models, the transition of model will be reflected on the variation of reside covariance. In other words, if there is a model transition, the residue covariance will produce a significant variation. We can use the hypothesis testing to judge the transition.

Based on the hypothesis testing theory [23], we define the null hypothesis H_0 and alternative hypothesis H_1 as:

$$H_0 : S_i = S_{i-1}, \ H_1 : S_i \neq S_{i-1}. \tag{30}$$

Therefore, we obtain the relation as the following:

$$\begin{aligned} &P\{\text{reject } H_0 \,|H_0 \text{ is true}\} \\ &= P\{(D_i \leq k_1) \cup (D_i \geq k_2)\} = s_h, \end{aligned} \tag{31}$$

where s_h is the significance level, k_1 and k_2 are the threshold values, $k_1 < k_2$.

According to above relation, we obtain the rejection region as follows:

$$D_i \leq k_1 = \chi^2_{1-s_h/2}(m) \quad or \quad D_i \geq k_2 = \chi^2_{s_h/2}(m). \tag{32}$$

Using the hypothesis testing, we evade the transition probability problem and judge the model transition of the system in the process of Kalman iteration. It is clear that the proposed scheme is an adaptive method to "switch" the model.

6.2 Clock Offset Tracking Using Multimodel Kalman Filter

From the scheme shown in the above section, we can see that the degree of freedom m and significance level s_h are the key parameters of tracking. For our clock, offset is the only observation data. Therefore, observation residue U_t is a one-dimensional vector, and $m = 1$.

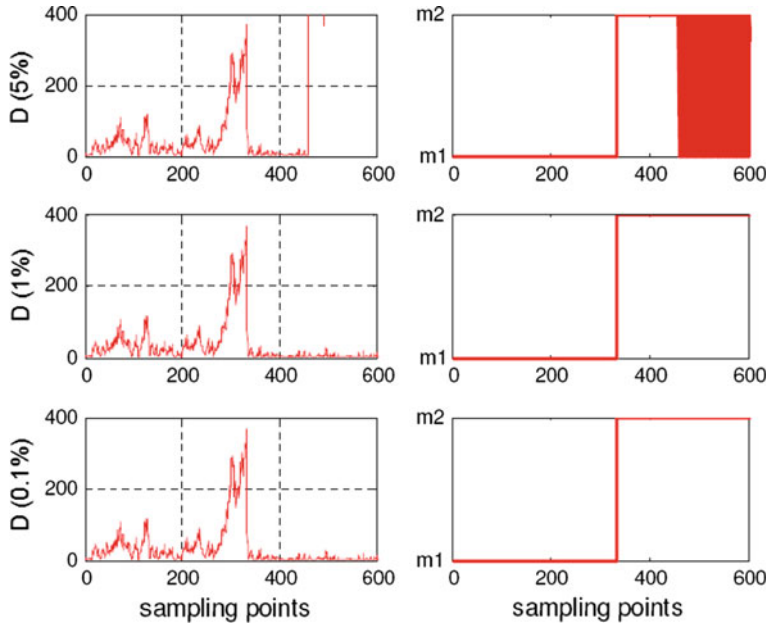

Fig. 9 Statistic value D_t and model switch situation for sensor1

For the hypothesis testing, popular levels of significance are 5, 1 and 0.1% [23]. If the significance has a probability value lower than the s_h-level, the null hypothesis is rejected. Smaller s_h-level gives greater confidence in the determination of significance, but it has greater risks of failing to reject a false null hypothesis (a Type II error, or "false negative determination" [23]), and hence it has less statistical power. The selection of a s_h-level inevitably involves a compromise between significance and power, and consequently between the Type I error and the Type II error. In our experiment, we implement a different test using 5, 1 and 0.1%, denoted as s_1, s_2, s_3 respectively. In addition, if the transition of model is smooth, we can adjust the significance levels to identify the switch in real experiment.

In our experiments, the initial model is the first-order model, since aging will not occur the first time. Figure 9 shows the statistic value of the D_i and model switch for sensor1 varying with time. From the left part of Fig. 9, we can see that there is a significant fluctuation at about the 300th sampling points even with different significance levels. It is clear that there is a model switch at this time. The right part of Fig. 9 shows the model switch situation in terms of $m1$ and $m2$, where $m1$ stands for the first-order model, and $m2$ stands for the second-order model. In addition, for the larger level (5%) part shown in the upper right of Fig. 9, there is an additional fluctuation compared to the other levels (1% and 0.1%). We can consider the additional fluctuation as the Type II error, since the level value is much larger than others.

Here we select level (1%) to verify the performance of multiple Kalman filtering as a simple example. Figure 10 shows the tracking performance by means of an error covariance matrix. We can see that $P(1, 1)$ converges to a stable value in a short time. There is a small fluctuation around 300th point, and it is reasonable that there is a model switch here. In conclusion, the multiple Kalman filter model demonstrates good convergence as shown in Fig. 10.

Figure 11 shows the error of estimation compared with observation value using different models. The error using the first-order model in the last life period and the error using the

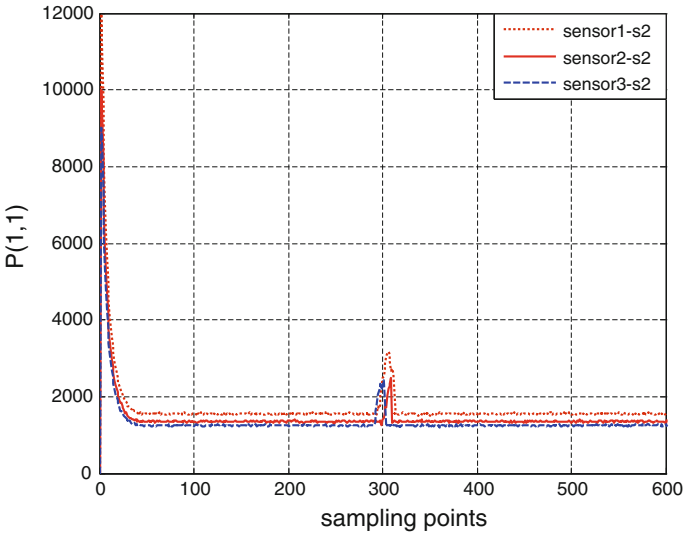

Fig. 10 The first entry of the error covariance matrix of clock offset tracking by using Multimodel

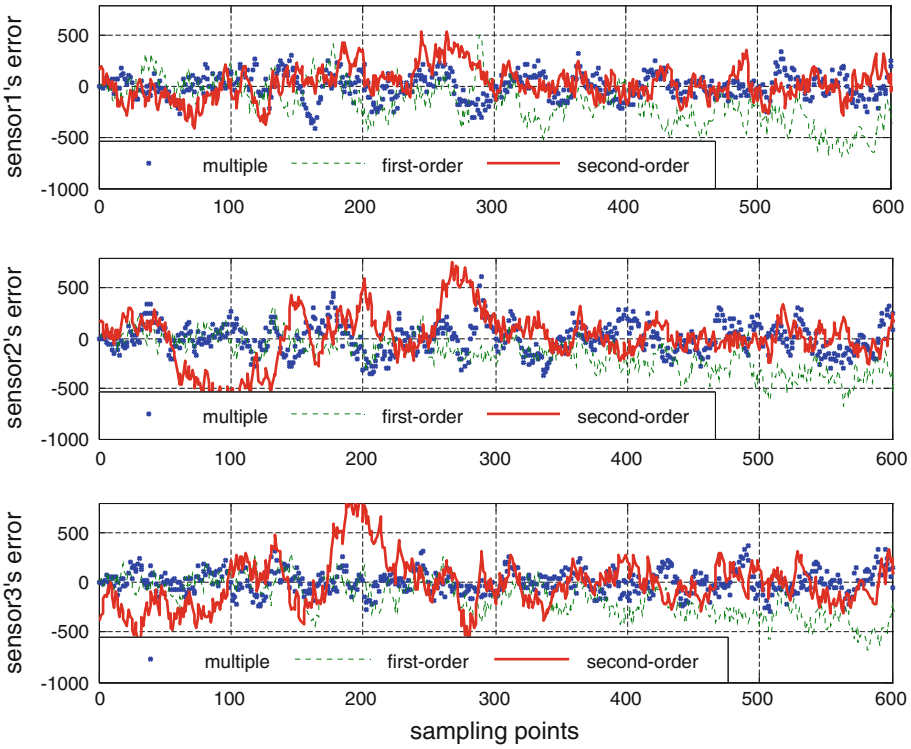

Fig. 11 Comparison of the error of different Kalman filer tracking

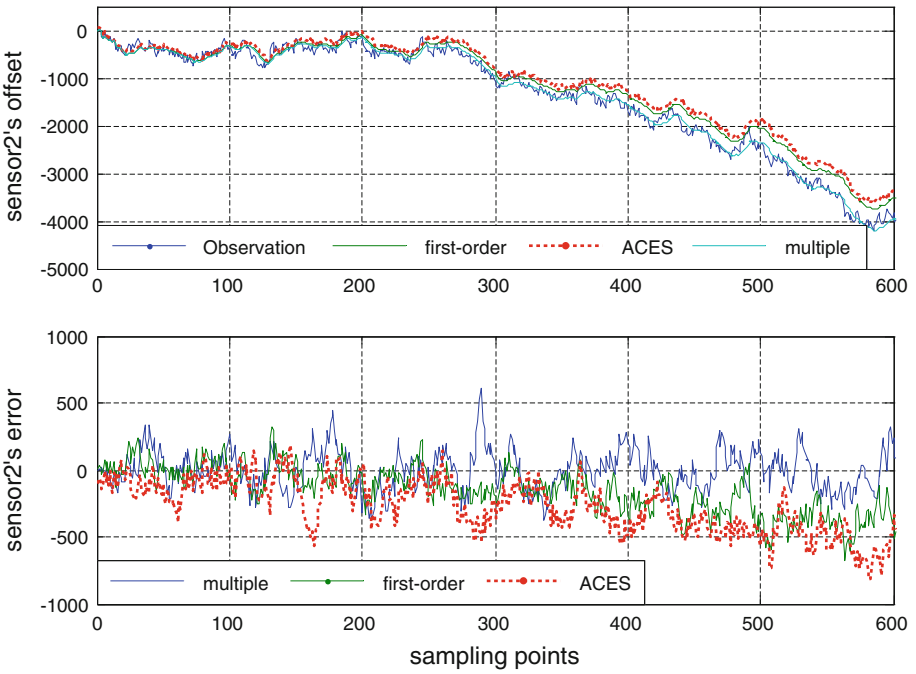

Fig. 12 Comparison of the error with ACES

second-order model in the first life period are larger than the the error using the Multimodel. It is clear that the Multimodel has much higher accuracy than the first-order and the second-order model.

6.3 Comparison with Other Scheme

To further demonstrate the performance of our scheme, we make a comparison with the method ACES proposed in [2].

According to ACES, we set the Kalman model for simulation as: $x = [o[n]\ s[n]]'$, $F = \begin{bmatrix} 1 & \tau \\ 0 & p \end{bmatrix}$, $H = [1\ 0]$. In addition, the state noise is $\mu[n] = [0\ \eta[n]]'$, and the observation noise is $\zeta[n]$. Here, p is the parameter of the AR(1) skew model: $s[k] = p \cdot s[k-1] + \eta[n]$, and p can be expressed as $p = \rho^{\tau/V}$. Furthermore, in order to implement the simulation, we set the parameters based on [2] as: $\rho = 1 - 2 \times 10^{-6}$, $V = 1$ h, $\sigma_\zeta^2 = (500 \times 10^3 \times 10^{-5})^2 = 25$, $\sigma_\eta^2 = (1 - p^2) \times (500 \times 10^3 \times 10^{-4})^2 = 0.5556$.

For simplicity, we use the data of sensor 2 to make the comparison in this paper. Figure 12 shows the error of estimation compared with observation value using Multimodel and ACES Kalman model [2]. From Fig. 12, we can see that there is the same tracking performance as the first-order model. It is reasonable because the parameter p in ACES model is a positive number less than but close to 1, in other words, the ACES model is close to the first model. In addition, the tracking performance of ACES is worse than the first-order model proposed in our paper because the parameters of model is set based on [2] instead of adaptive estimating.

Note that, the method shown in [2] use the simulation to demonstrate the performance, but we use the practical experiment to achieve the demonstration in this paper.

7 Conclusion

Efficient and accurate time synchronization is a challenge for resource-constrained WSNs. This paper examines the clock synchronization scheme using different Kalman filter models and various experiments. According to these experiments on WSN sensors, we propose a general clock model to describe the desynchronization of the clock in terms of the oscillator, and we design two kinds of basic Kalman filter models to track clock offset. We also apply the EM algorithm to adaptively estimate the Kalman model's parameter based on experiment data. To increase accuracy, we propose a multiple Kalman filter model based on the practical clock offset rule and experiments on single models. Furthermore, we apply the hypothesis testing to address the challenge of model switch. According to the results of all the schemes implemented based on experiment data, we make the conclusion that the general Multimodel Kalman filter proposed in our paper achieves higher synchronization accuracy than the first-order, the second-order models and ACES model. In addition, the adaptive parameter estimation and model switch method make the scheme achieve higher application value.

References

1. Veitch, D., Ridoux, J., & Korada, S. B. (2009). Robust synchronization of absolute and difference clocks over networks. *IEEE/ACM Transactions on Networking (TON), 17*(2), 417–430.
2. Hamilton, B. R., Ma, X., Zhao, Q., & Xu, J. (2008). Aces: adaptive clock estimation and synchronization using kalman filtering. In *Proceedings of the 14th ACM international conference on mobile computing and networking, MobiCom 2008* (pp. 152–162).
3. Sommer, P., & Wattenhofer, R. (2009). Gradient clock synchronization in wireless sensor networks. In *Proceedings of the 8th ACM/IEEE international conference on Information Processing in Sensor Networks, IPSN*.
4. Sundararaman, B., Buy, U., & Kshemkalyani, A. D. (2005). Clock synchronization for wireless sensor networks: A survey. *Ad Hoc Networks, 3*(3), 281–323.
5. Mudumbai, R., Barriac, G., & Madhow, U. (2007). On the feasibility of distributed beamforming in wireless networks. *IEEE Transactions on Wireless Communications, 6*(5), 1754–1763.
6. Capkun, S., Cagalj, M., Srivastava, M. (2006). Secure localization with hidden and mobile base stations. In *Proceedings of 25th IEEE international conference on computer communications, INFOCOM* (pp. 1–10).
7. Mills, D. L. (1991). Internet time synchronization: The network time protocol. *IEEE Transactions on Communications, 39*(10), 1482–1493.
8. Elson, J.E. (2003). Time synchronization in wireless sensor networks, Ph.D. thesis, University of California Los Angeles.
9. Galleani, L., Sacerdote, L., Tavella, P., & Zucca, C. (2003). A mathematical model for the atomic clock error. *Metrologia-Berlin, 40*(3), 257–264.
10. Kim, K. S., & Lee, B. G. (2000). Kalp: A kalman filter-based adaptive clock method with low-pass prefiltering for packet networks use. *IEEE Transactions on Communications, 48*(7), 1217–1225.
11. Auler, L. F., & d'Amore, R. (2007). Adaptive kalman filter for time synchronization over packet-switched networks: An heuristic approach. In *IEEE COMSWARE 2007* (pp. 1–7).
12. Veitch, D., Babu, S., & Psztor, A. (2004). Robust synchronization of software clocks across the internet. In *Proceedings of the 4th ACM SIGCOMM conference on internet measurement* (pp. 219–232).
13. Allan, D. W. (1987). Time and frequency (time-domain) characterization, estimation, and prediction of precision clocks and oscillators. *IEEE Transactions on Ultrasonics, Ferroelectrics and Frequency Control, 34*(6), 647–654.
14. Sullivan, D., Allan, D., Howe, D., & Walls, F. (1990). Characterization of clocks and oscillators, Tech. rep., National Inst. of Standards and Technology, Boulder, CO. Time and Frequency Div.
15. Pottie, G., & Kaiser, W. (2000). Wireless integrated network sensors. *Communications of ACM, 43*(5), 51–58.
16. Kalman, R. E. (1960). A new approach to linear filtering and prediction problems. *Journal of Basic Engineering, 82*(1), 35–55.

17. Kalman, R. E., & Bucy, R. S. (1973). New results in linear filtering and prediction theory. *Random Processes, 15*, 181–190.
18. Tie, Y., & Guan, L. (2009). Automatic face detection in video sequences using local normalization and optimal adaptive correlation techniques. *Pattern Recognition, 42*(9), 1859–1868.
19. Shumway, R. H., & Stoffer, D. S. (1982). An approach to time series smoothing and forecasting using the em algorithm. *Journal of Time Series Analysis, 3*(4), 253–264.
20. Dempster, A. P., Laird, N. M., Rubin, D. B. (1977). Maximum likelihood from incomplete data via the em algorithm. *Journal of the Royal Statistical Society. Series B* (Methodological) 1–38.
21. Bar-Shalom, Y., & Li, X. R. (1995). *Multitarget-multisensor tracking: Principles and techniques*. Storrs, CT: University of Connecticut.
22. Li, X. R., Zhao, Z., & Li, X. B. (2005). General model-set design methods for multiple-model approach. *IEEE Transactions on Automatic Control, 50*(9), 1260–1276.
23. Lehmann, E. L. (2005). *Testing statistical hypotheses* (3rd ed.). New York: Springer.

Author Biographies

Qiang Liu is a Ph.D. student of College of Information System and Management in National University of Defense and Technology, China. He is also a join-student of School of Computer Science at McGill University, Canada. Currently he is mainly interesting in wireless sensor networks, system pattern recognition, system reliability, Bayesian method, and prognostics and health management.

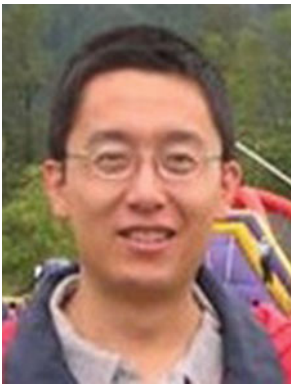

Xue Liu is a Ph.D. and an associate professor of McGill University, Canada. His research interests are wireless sensor networks, cyber-physical systems, real-time and embedded systems.

Jing Lun Zhou is a Ph.D. and a professor of National University of Defense Technology, China. His research interests are system reliability, risk assessment and evaluation, information management and decision, failure diagnostics, and prognostics and health management.

Gang Zhou is a Ph.D. and an assistant professor of College of William and Mary, USA. His research interests are wireless sensor networks, cyber-physical systems, wireless communication and networking, and underwater sensor networks.

Guang Jin is a Ph.D. and an associate professor of National University of Defense Technology, China. His research interests are system modeling and simulation, system reliability estimation, experiment and evaluation, and prognostics and health management.

Quan Sun is a Ph.D. and an associate professor in National University of Defense Technology, China. He is also a visiting scholar of School of Industrial and Systems Engineering at Georgia Institute of Technology, USA. His research interests are risk assessment and evaluation, physics of reliability, and failure diagnostics.

Min Xi is a Ph.D. and a lecturer of Xi'an Jiaotong University, China. His research interests are system modeling and simulation, complex wireless sensor network, and failure diagnostics.